Energy-partition diagnostic for measuring time-resolved scattering and absorption in burst-mode laser ablation

Z. Qian,[1] J. E. Schoenly,[1] A. Covarrubias,[1] L. Lilge,[2] and R. S. Marjoribanks[1,a)]
[1]*Department of Physics and Institute for Optical Sciences, University of Toronto, Toronto M5S 1A7, Canada*
[2]*Princess Margaret Cancer Centre and Department of Medical Biophysics, University of Toronto, Toronto M5G 1L7, Canada*

(Received 17 December 2013; accepted 10 February 2014; published online 3 March 2014)

We describe an energy-partition diagnostic based on integrating sphere principle for measuring absorption and scattering in plasma-mediated ablation by a high repetition-rate (133 MHz), pulsetrain-burst ultrafast-pulse laser. The system time-resolves the partition of elastically scattered laser light into specular reflection, diffuse reflection, and transmission, giving access to per-pulse absorption dynamics. Physical events such as optical breakdown and incubation effects in glass and aluminum are illustrated. © *2014 AIP Publishing LLC*. [http://dx.doi.org/10.1063/1.4866658]

I. INTRODUCTION

Plasma-mediated ablation by ultrafast laser pulses has been widely investigated and used in non-contact materials-processing,[1] surgery,[2,3] and research.[4] Delivering the pulses in bursts (i.e., packets of pulses) with a fixed, short inter-pulse separation[5] offers new controls over repetition rate and pulsetrain length. Pulsetrain-burst mode ultrafast lasers have demonstrated advantages of finer ablation, and higher material removal efficiency compared to lower repetition rate ultrafast lasers.[3,6,7]

Optimization of this additional parameter space relies on detailed investigation of the physical mechanisms for ablation (e.g., optical breakdown, cavitation, shockwave, etc.), which depend on the absorption of laser-pulse energy.[4,8–12] Hence, studying absorption provides vital guidance to maximize ablation rates while minimize collateral damage due to thermal or mechanical stresses.

Different from the low repetition-rate case, absorption of high repetition-rate (>100 MHz) pulsetrain-bursts is a dynamic process across not only short time scales (femtosecond to picosecond pulsewidths, and nanoseconds of inter-pulse separation), but also long (microseconds of pulsetrain length) time scales. In a pulsetrain where the inter-pulse separation is several nanoseconds, any pulse can interact with residual plasma created or sustained by previous pulses. Besides critical-density plasma near the solid surface, a plume of ejected material persists, which consists of plasma and potentially of nanoparticles, which will absorb, scatter, and reflect laser light, preventing some fraction of laser energy from reaching the target.[13,14] (In our case, the precise contribution of nanoparticles is unclear—significant heating by pulses arriving every 7.5 ns in the plume will to some degree alter the conditions which are known to produce nanoparticles for lower repetition-rate irradiation.) Thus, absorption of a given pulse depends on the history of previous pulses. Moreover, development of an ablation crater or the expansion/collapsing of a cavitation bubble in a soft material also contributes to the dynamics of absorption throughout a pulsetrain. Therefore, characterizing the absorption of pulsetrain-bursts by solid target material and its plume requires a diagnostic device that time-resolves the absorption of each pulse.

Previously, researchers have measured absorption of single-pulse or low repetition-rate (kHz) pulses, using approaches including direct measurement by calorimetry[15,16] and indirect measurement by inferring the absorption from the difference between the incident energy and the scattered and reflected energy.[9–12,17–19] However, when it comes to characterizing high-repetition pulsetrain absorption: calorimetry does not offer sufficient temporal resolution to time-resolve the absorption of each pulse. On the other hand, previous indirect measurements were not capable of making a full energy inventory over all solid angles, for sufficient time, and with sufficient resolution to study burst-mode laser ablation.

Developed in the 19th century,[20,21] the integrating sphere or cavity is an established device used in a variety of optical measurements.[22–26] It offers an indirect measurement of absorption by collecting all of the scattered light and inferring plasma absorption as the difference between the incident energy and the elastic scattered energy.[24]

This article describes a diagnostic tool based on integrating sphere principle that collects the laser light scattered in plasma-mediated ablation into 4 different spatial compartments, therefore allowing indirect measurement of absorption. The diagnostic also has sufficient temporal resolution to measure absorption of each pulse in a 133 MHz repetition-rate pulsetrain.

II. THE ENERGY-PARTITION DIAGNOSTICS

The laser used in this study is a 1053 nm, 1.5 ps pulsewidth, Nd:glass pulsetrain-burst-mode laser (Figure 1), described previously.[6,27] The laser beam was focused on the target to a ∼5 μm diameter spot, using a 20-mm-focal-length aspherical lens (f-number of beam: *f*/2.0). Focusing was verified by imaging onto an equivalent target plane (ETP).

In plasma-mediated ablation, light scatters or reflects anisotropically from the plasma. So the energy-partition

a)Author to whom correspondence should be addressed. Electronic mail: marj@physics.utoronto.ca

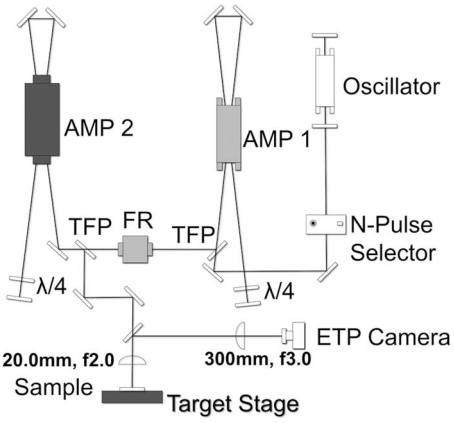

FIG. 1. Schematic of the pulsetrain-burst mode ultrafast laser system, showing amplifiers (AMP 1, AMP 2); Faraday rotator (FR); thin film polarizer (TFP); quarter waveplate (λ/4); and equivalent target plane (ETP).

diagnostic collected specular reflection, diffuse reflection, and transmission in four different compartments using a variety of integrating cavities.

Due to the high reflectivity of dense plasma, a significant fraction of the incident light will be specular- or diffuse-reflected, so a specular-reflection integrator (SRI) was placed onto the equivalent-target-plane (ETP) path (see Figure 2), while a diffuse-reflection integrator (DRI) quantified the reflection coming from angles 4° and 32°. In addition, an upper sphere (US) measured the remaining diffuse reflection in the upper hemisphere, and a lower sphere (LS) measures transmission of angles from 90° to 180°. Each component was created either out of a sphere or a tube with its interior painted with high reflectance coating (Avian-B^{TM}, Avian Technologies, LLC). The reflectivity of the coating at 1053 nm is 97.8%.

All components are equipped with 1-ns-rise-time photodiodes, and signals are recorded using GS/s sampling rate oscilloscopes (TDS3044B, 5GS/s, 400 MHz, Tektronix, and WaveSurfer 454, 2 GS/s, 500 MHz, LeCroy). A 1050 nm bandpass filter with 10 nm bandwith (Stock # 65-769, Edmund Optics, OD ≥ 4) and a FGL1000 (Thorlabs, OD ≥ 3)

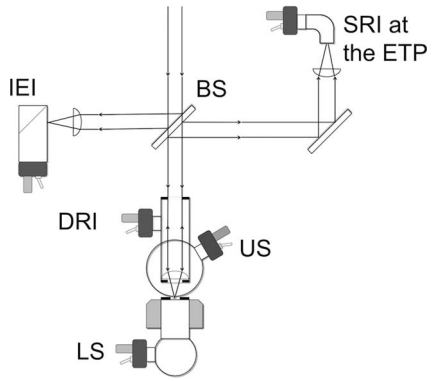

FIG. 2. Schematic of the time-resolving energy-partition diagnostic. SRI: 1-in. long, 1/2-in.-diameter integrating tube at the ETP; DRI: 1-in. diameter, 3-in.-long integrating tube with a 0.5-in. aperture on each end; US: 2-in.-diameter integrating sphere; LS: 1.5-in. diameter integrating sphere; IEI: 2-in. long, 1-in. diameter integrating tube; and BS: 90/10 beam-splitter.

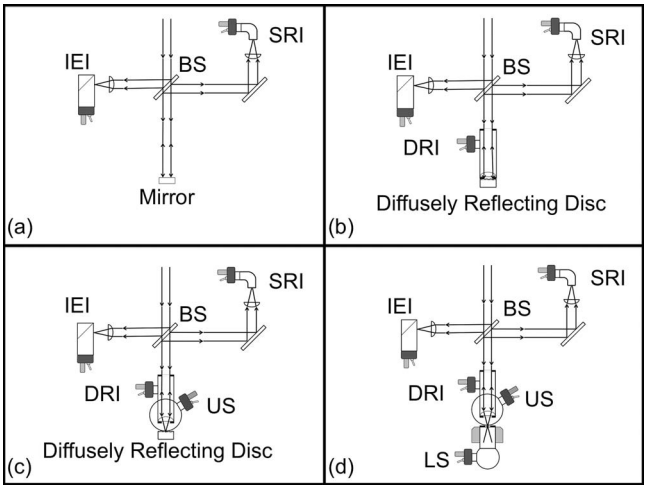

FIG. 3. Steps in calibration of each component. (a) SRI: the US and the DRI were removed. A mirror (BB1-E03P, Thorlabs) resulted in 99% specular reflection of the incident energy. (b) DRI: a disc with high reflectance coating sealed the lower aperture of the DRI, resulting in a 97.8% diffuse reflection. (c) US: the disc with high reflectance coating sealed the lower aperture of the US, resulting in a 97.8% diffuse reflection (d) LS.

long pass filter were installed on each detector port. Calibration of each component's collection efficiency is presented in Sec. III.

In addition, an incident energy integrator (IEI), calibrated against a power meter quantifies the pulse energy of the incident radiation.

III. CHARACTERIZING OF THE DOUBLE INTEGRATING SPHERES

A. Calibration of collection efficiency

Calibration of collection efficiency was achieved by sending a known fraction of the incident energy sequentially to each "to be calibrated" component (see Figure 3 for steps).

Each component's calibration factor was calculated based on more than 1000 pulses at different intensities. The responsivity of each component followed a linear fit (Figure 4).

It is convenient to describe responsivity as the ratio between signal peak and pulse energy, which is shown in Table I. The detection limit of each component was defined as the energy corresponding to the minimum detectable signal peak (1-mV pulse) of the photodiodes.

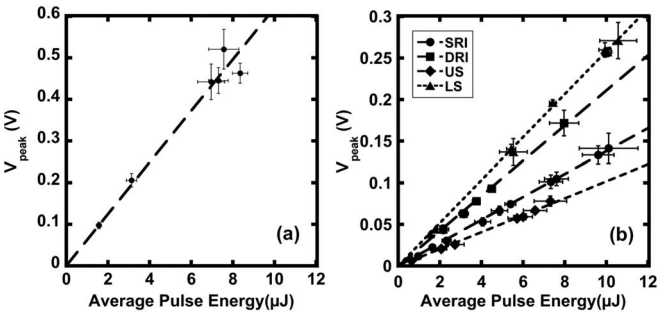

FIG. 4. Responsivity of: (a) IEI and (b) SRI, DRI, US, and LS.

TABLE I. Characterization of the double-integrating-sphere system.

	IEI	SRI	DRI	US	LS
Responsivity (mV/μJ)	63 ± 4	13 ± 1	21 ± 1	10 ± 1	25 ± 1
Detection limit (nJ)	15 ± 1	74 ± 3	49 ± 1	102 ± 4	39 ± 1
1/e rise time (ns)	0.8 ± 0.7	0.6 ± 0.1	0.9 ± 0.1	1 ± 0.1	0.9 ± 0.1
1/e fall time (ns)	3.1 ± 0.2	1.5 ± 0.1	1.9 ± 0.1	2.0 ± 0.1	1.7 ± 0.1

The temporal response of each component was measured by the widths of the response signal following exposure of 1.5 ps impulse (Table I). The FWHM of components ranges from 1.6 to 2.6 ns, which is adequate to time-resolve pulses of 7.5 ns inter-pulse separation. However, the temporal evolution of absorption during each pulse, such as initiation of a plasma cannot be resolved. The timebase registration, or synchronization, of all channels was established using a single-pulse dataset.

B. Artifacts within the system

Unintended reflection from optics created artifacts within the system, and these artifacts had to be characterized for accurate interpretation of the absorption data. Artifacts within the system include: reflection from the glass sample holder between the two spheres into the US; reflection from the lens of the IEI into the SRI; and the reflection of the aspherical lens into the DRI. These artifacts are taken into account when quantifying scattering and absorption in Sec. IV.

IV. ILLUSTRATION OF TIME-RESOLVED ABSORPTION MEASUREMENT OF ALUMINUM FOIL AND GLASS

Examples of this partition diagnostic for a time-resolved measurement of absorption are given when ablating a thin aluminum foil and a glass microscope slide with pulsetrain bursts.

A 53-μm-thick aluminum foil was ablated with a 10 μs pulsetrain consist of 1333 separate 1.5 ps pulses at 3×10^{13} W cm^{-2}. (Only the first 230 pulses are shown due the recording length of the oscilloscope.) As pulses perforated the foil after 300 ns, the transmission rose from 0 to ~50% in 9 pulses, then continued to increase to ~80% in 93 pulses (Figure 5(a)). Reflection commenced with ~23% specular reflection and ~8% diffuse reflection (Figure 5(b)), then specular and diffuse reflection dropped to 0% and ~2% of the incident energy, respectively.

As a result, absorption immediately rose from ~50% to between 80% and 90% after the first 1–2 pulses. The absorption remained high for ~500 ns, until the laser pulses drilled through the aluminum, after which most of the laser energy was transmitted into the lower sphere.

Prior to the perforation of the foil, laser light was scattered, reflected, and absorbed both by the foil and by the plume of ejected material. The perforation of the foil produced the sudden rise of transmission to ~50% at ~500 ns into the pulsetrain. Then the subsequent gradual rise of the transmission from 50% to 80% after drilling the foil likely has two contributions: gradual enlargement of the perforated hole (which may clip the focal spot edges or block light scattered by small angles in the plume); and slow reduction of absorption in the established plume created by previous pulses, as ablated material no longer flows backward into the plume.[28] Therefore, we conclude that during ablation absorption in the plume is less than 30% of laser energy, while the foil absorbs more than 60%.

Dielectrics (e.g., glass) have a distinction from metals in that they have virtually no free electrons prior to laser irradiation, to mediate absorption. High-irradiance ultrafast laser pulses produce multi-photon absorption or tunnel ionization, immediately followed by avalanche ionization, so laser-induced optical breakdown occurs rapidly for such pulses in dielectrics.

Figure 6(a) shows the time-resolved transmission, reflection, and absorption of 1-mm-thick glass microscope slide (Goldline™ Extra White (clear, low-iron, soda-lime glass) microscope slides, VWR LLC) when ablated with 10 μs pulsetrain at 1×10^{13} W cm^{-2}. Transmission of glass was ~80% at the onset of the pulsetrain, until plasma was initiated on the surface of the glass after ~500 ns. Due to direct

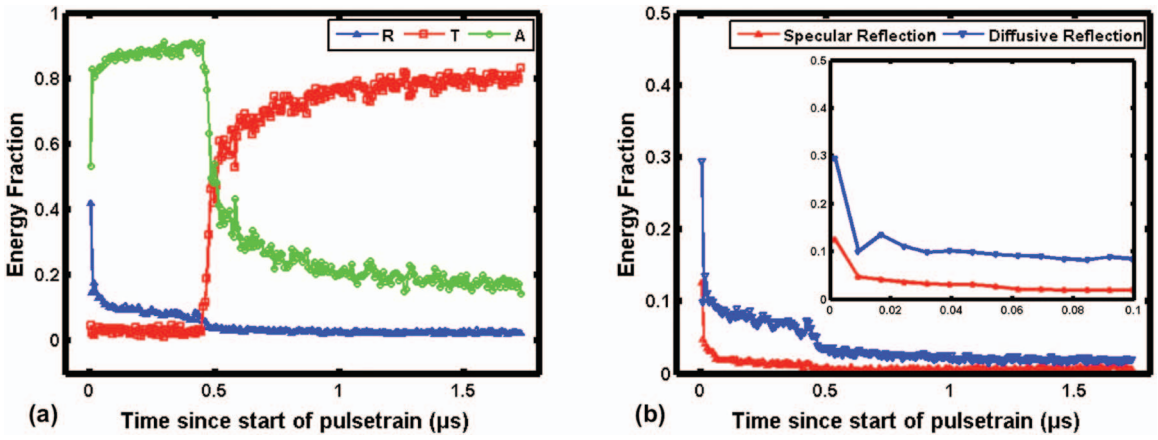

FIG. 5. (a) Time-resolved total reflection (R), transmission (T), and absorption (A) of 53 μm thick aluminum foil when ablated with 10 μs pulsetrain of 1.5 ps pulses at 3×10^{13} W cm^{-2}. (Only the first 230 pulses are shown.) (b) Time-resolved specular and diffuse reflection of 53 μm thick aluminum foil when ablated with 10 μs pulsetrain of 1.5 ps pulses at 3×10^{13} W cm^{-2}. The inset shows the specular and diffuse reflection in the first 0.1 μs of the pulsetrain. (Only the first 230 pulses are shown in the figure.)

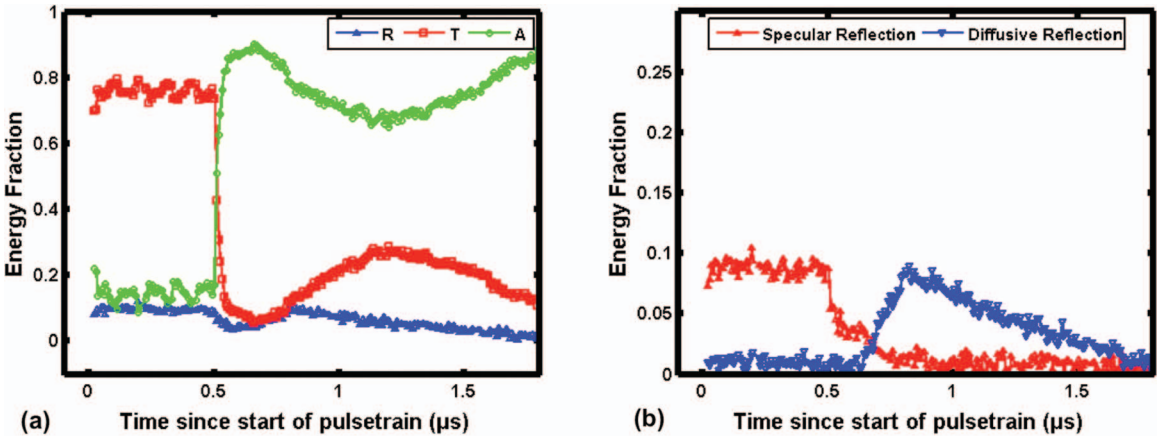

FIG. 6. (a) Time-resolved reflection (R), transmission (T), and absorption (A) of 1 mm glass microscope slide when ablated at 1×10^{13} W cm^{-2}. The plasma was initiated on the surface of the glass after ~500 ns. (b) Time-resolved specular and diffuse reflection of 1 mm glass microscope slide during ablation by 10 μs pulsetrains of 1.5 ps pulses at 1×10^{13} W cm^{-2}. (Only the first 230 pulses are shown in the figure.)

absorption by the plasma and shielding by an ablation plume, the transmission dropped to ~20%, where it remained for the balance of the pulsetrain.

Total reflection shows a more complex temporal behavior, which can be understood by further examining specular and diffuse reflection (Figure 6(b)). At the beginning of the pulsetrain, the glass surface was intact and the specular reflection was ~7% and diffuse reflection close to 0%. Once optical breakdown began, specular reflection decreased, while diffuse reflection increased. This was presumably due to the expansion of plasma, as well as reflection by the critical density electron near the convex ablated surface.

Consequently, absorption rose from ~10% to 80% once the breakdown was initiated, then it varied between 70% and 90% throughout the later part of the pulsetrain. The exact mechanisms that resulted in such variance were not further addressed for this paper.

The above two examples demonstrate that the energy-partition diagnostic is capable of time-resolving the absorption of pulsetrain-burst laser ablation, and that such capability offers important insight to the dynamics of the plasma-mediated ablation process.

V. CONCLUSION

The energy-partition diagnostic is purpose-built to time-resolve absorption during burst-mode ultrafast-laser ablation. Detailed calibration shows the diagnostic has sufficient sensitivity and temporal resolution for time-resolving pulsetrains that operates at 133 MHz repetition rate.

As demonstrated in examples in glass and metal, pulsetrain ablation is a dynamic process. Reflection, transmission, and absorption undergo drastic change during the pulsetrain on a nanoseconds timescale. Capturing such rapid change raises challenges to the previous methods of absorption measurement: While the calorimetry method provides the total energy absorption of ablation by measuring the temperature change of the target before and after ablation, it does not provide the time-resolved information on how absorption varies throughout the pulsetrain. On the other hand, to time-resolve the pulsetrain ablation using the pump-probe method, one has to carry out repeated trials at different time-delays between the pump and the probe pulse, assuming that laser parameters remain identical in these different trials. The energy-partition diagnostic complements the previous methods with its capability of continuous recording at high temporal resolution, so that the dynamic reflection, scattering, and absorption can be captured. Although the apparatus is specifically designed for pulsetrain-burst mode ultrafast lasers, it is also applicable to better study the dynamics of plasma-mediated ablation in general.

ACKNOWLEDGMENTS

This work was supported by the Natural Sciences and Engineering Research Council of Canada (NSERC).

[1]R. R. Gattass and E. Mazur, Nat. Photon. **2**, 219 (2008).
[2]T. Juhasz, F. H. Loesel, and R. M. Kurtz, IEEE J. Sel. Top. Quantum Electron. **5**, 902 (1999).
[3]K. Koenig, O. Krauss, and I. Riemann, Opt. Express **10**, 171 (2002).
[4]A. Vogel, J. Noack, G. Hüttman, and G. Paltauf, Appl. Phys. B: Lasers Opt. **81**, 1015 (2005).
[5]P. R. Herman, R. Marjoribanks, and A. Oettl, U.S. Patent No. 6,552,301 (2003).
[6]R. S. Marjoribanks, C. Dille, J. E. Schoenly, L. McKinney, A. Mordovanakis, P. Kaifosh, P. Forrester, Z. Qian, A. Covarrubias, Y. Feng, and L. Lilge, Photon. Lasers Med. **1**, 155 (2012).
[7]M. Lapczyna, K. P. Chen, P. R. Herman, H. W. Tan, and R. S. Marjoribanks, Appl. Phys. A: Mater. Sci. Process. **69**, S883 (1999).
[8]A. Vogel and V. Venugopalan, Chem. Rev. **103**, 577 (2003).
[9]A. Vogel, J. Noack, K. Nahen, D. Theisen, S. Busch, U. Parlitz, D. X. Hammer, G. D. Noojin, B. A. Rockwell, and R. Birngruber, Appl. Phys. B: Lasers Opt. **68**, 271 (1999).
[10]J. Noack and A. Vogel, IEEE J. Quantum Electron. **35**, 1156 (1999).
[11]A. Vogel, K. Nahen, and D. Theisen, IEEE J. Sel. Top. Quantum Electron. **2**, 847 (1996).
[12]K. Nahen and A. Vogel, IEEE J. Sel. Top. Quantum Electron. **2**, 861 (1996).
[13]S. Amoruso, R. Bruzzese, C. Pagano, and X. Wang, Appl. Phys. A **89**, 1017 (2007).
[14]D. Rioux, M. Laferrière, A. Douplik, D. Shah, L. Lilge, A. V. Kabashin, and M. M. Meunier, J. Biomed. Opt. **14**(2), 021010 (2009).
[15]A. Y. Vorobyev and C. Guo, Appl. Phys. Lett. **86**, 011916 (2005).
[16]A. Vorobyev and C. Guo, Phys. Rev. B **72**, 195422 (2005).

[17]D. Puerto, J. Siegel, W. Gawelda, M. Galvan-Sosa, L. Ehrentraut, J. Bonse, and J. Solis, J. Opt. Soc. Am. B **27**, 1065 (2010).
[18]J. Hernandez-Rueda, D. Puerto, J. Siegel, M. Galvan-Sosa, and J. Solis, Appl. Surf. Sci. **258**, 9389 (2012).
[19]C. B. Schaffer, N. Nishimura, E. N. Glezer, A. Kim, and E. Mazur, Opt. Express **10**, 196 (2002).
[20]J. A. Jacquez and H. F. Kuppenheim, J. Opt. Soc. Am. **45**, 460 (1955).
[21]D. G. Goebel, Appl. Opt. **6**, 125 (1967).
[22]S. A. Prahl, M. Van Gemert, and A. J. Welch, Appl. Opt. **32**, 559 (1993).
[23]J. Pickering, C. Moes, H. Sterenborg, S. A. Prahl, and M. Van Gemert, J. Opt. Soc. Am. A **9**, 621 (1992).
[24]L. Hanssen, Appl. Opt. **40**, 3196 (2001).
[25]A. Roos, Solar Energy Mater. Solar Cells **30**, 77 (1993).
[26]K. Shiokawa, Y. Katoh, M. Satoh, M. K. Ejiri, and T. Ogawa, Adv. Space Res. **26**, 1025 (2000).
[27]R. S. Marjoribanks, F. W. Budnik, L. Zhao, and G. Kulcsar, Opt. Lett. **18**, 361 (1993).
[28]J. Dean, M. Bercx, F. Frank, R. Evans, S. Camacho-Lopez, M. Nantel, and R. Marjoribanks, Opt. Express **16**, 13606 (2008).